Well-Defined Liquid-Crystalline Diblock Copolymers with an Azobenzene Moiety: Synthesis, Photoinduced Alignment and their Holographic Properties

Haifeng Yu, Yumiko Naka, Atsushi Shishido, and Tomiki Ikeda*

Chemical Resources Laboratory, Tokyo Institute of Technology, R1-11, 4259 Nagatsuta, Midori-ku, Yokohama 226-8503, Japan

Received May 14, 2008; Revised Manuscript Received August 28, 2008

ABSTRACT: A series of liquid-crystalline (LC) diblock copolymers with an azobenzene moiety in the side chain were prepared by atom transfer radical polymerization (ATRP). Using a bromo-terminated poly(methyl methacrylate) as a macroinitiator, the obtained diblock copolymers showed well-defined structures and narrow molecular-weight distributions. Microphase-separated nanostructures with mesogenic blocks in either continuous or separated phases were observed. Owing to varied content of mesogens in the block copolymers, they showed different behavior of photoinduced alignment and holographic recording. Block copolymers with azobenzenes in the majority phases exhibited a similar performance of photoinduced alignment and refractive-index modulation to the azobenzene-containing homopolymer, but their photoinduced mass transportation was partly suppressed by the microphase separation, leading to a lower surface relief than that of the homopolymer. The photoinduced mass transfer was greatly prohibited in the block copolymers with mesogenic groups in the minority phases, resulting in little surface relief. However, refractive-index gratings were still recorded upon local alignment, driven by the photoinduced alignment of azobenzenes or the phototriggered molecular cooperative motion between azobenzenes and nonphotosensitive cyanobiphenyl groups. Then the possible schematic illustrations of mesogens and microphase separation in the grating structures were proposed.

1. Introduction

Liquid-crystalline (LC) block copolymers (BCs) with well-defined structures combine nanoscaled microphase separation of BCs with excellent characteristics of LC polymers (LCPs),[1,2] enabling them to show diverse nanostructures such as spheres, cylinders, and lamellae,[3] as well as self-organizing nature of long-range order, fluidity, cooperative motion (CM) and anisotropy in various physical properties.[2] In the process of microphase separation, the regular periodicity of LC ordering has a great influence on the microphase-separated nanostructures, making it possible to self-assemble into periodic nanostructures at a macroscopic scale.[4−6] The interplay process between the microphase separation and the additional elastic deformation of LC ordering, called as supramolecular CM,[4] provides a novel opportunity to control ordered nanostructures. Especially, azobenzene (AZ)-containing LCPs, in which the AZ moiety plays both roles as a mesogen and a photosensitive chromophore,[2] have been introduced, giving the LCBCs novel photocontrol properties under the function of supramolecular CM.[4,5]

Eliminating the scattering of visible light, the nanoscaled microphase separation provides the LCBCs with versatile optical applications such as improved stability of photoinduced birefringence,[7a] physical cross-links of thermoplastic elastomers,[7b] and confinement effect on the photoalignment, photochemical phase transition and thermochromic behavior.[7c] Recently, we reported an enhancement effect of surface-relief gratings (SRGs) in a novel amphiphilic LCBC consisting of flexible poly(ethylene oxide) (PEO) as a hydrophilic segment and polymethacrylate containing an AZ moiety in the side chain as a hydrophobic LC block.[5b] Upon thermally enhanced microphase separation, the diffraction efficiency of the inscribed gratings was drastically increased by 2 orders of magnitude, indicating its potential application in secure holographic storage.[5b] But the hydrophilicity and low glass-transition temperature (T_g) of PEO limit its utilization as recording media. To improve the stability, polystyrene (PS) has been used as one constituent block to design BCs with holographic recording functions.[8] However, the refractive-index modulation in the grating formation was very low as the PS-based BCs prepared by Schimidt et al. did not show LC properties.[8] In order to integrate the excellent feathers of LCPs with holographic properties of AZ-containing BCs, we designed a series of poly(methyl methacrylate) (PMMA)-based LCBCs with AZs or cyanobiphenyl groups (CBs) as mesogens. Generally, amorphous PMMA has good optical transparency[9,10] and its T_g is similar to that of PS. In this paper, we report the synthesis of PMMA-based LCBCs with well-defined structures by atom transfer radical polymerization (ATRP) and their photoinduced alignment behavior as well as holographic properties.

2. Experimental Section

2.1. Measurements. ^{1}H NMR spectra were measured using a Lambda-300 spectrometer operating at 300 MHz with tetramethylsilane as an internal reference for chemical shifts. Molecular weights of the polymers were determined by gel permeation chromatography (GPC, JASCO) and referenced against standard PSs with chloroform as eluent. They were also calculated by ^{1}H NMR method to make sure the results are correct. The thermodynamic properties of the monomers and the polymers were analyzed with a differential scanning calorimeter (DSC, Seiko) at a heating and cooling rate of 10 °C/min. At least three scans were performed to check the reproducibility. The LC properties were evaluated with a polarizing optical microscope (POM, Olympus BH-2). The UV−vis absorption spectra were measured in a film or a chloroform solution using a JASCO V-550 spectrophotometer. Atomic force microscopy (AFM) images of surface modulation in a tapping mode were detected with a scanning probe microscope (Veeco Instruments Inc., Nanoscope IV) at room temperature.

2.2. Materials. To get rid of a stabilizer (hydroquinone, 0.005%) in commercially available methyl methacrylate (MMA, 98%), MMA was washed twice with an aqueous solution of sodium hydroxide (5%) and twice with distilled water, then stirred over

* Corresponding author. E-mail: tikeda@res.titech.ac.jp. Telephone: +81-45-924-5240. Fax: +81-45-924-5275.

10.1021/ma801077g CCC: $40.75
Published on Web 10/08/2008

CaH_2 overnight and distilled under vacuum prior to polymerization. Ethyl 2-bromoisobutyrate (EBrIB), triethylamine, methacryloxy chloride, triethylamine, 4-cyano-4′-hydroxybiphenyl, 6-chloro-1-hexanol, *N*,*N*-dimethylformamide (DMF), 4-ethoxylaniline and hydroquinone were commercially available (Kanto Chem. Co.) and used without further purification. Anisole and tetrahydrofuran (THF) were purified by distillation from sodium with benzophenone. The ligand, 1,1,4,7,10,10-hexamethyltriethylenetetramine (HMTETA, Aldrich) was used as received without further purification. The catalyst $Cu^{I}Cl$ was washed successively with acetic acid and ether, then dried. 2,2′-Azobis(isobutyronitrile) (AIBN, Wako Pure Chem.) was recrystallized from anhydrous methanol.

2.3. Synthesis of Monomers and Polymers. *6-(4-(4-Ethoxyphenylazo)phenoxy)hexyl methacrylate (M6AB).* The monomer M6AB was prepared by a diazo-coupling reaction between 4-ethyoxylaniline and phenol in the presence of sodium nitrite and hydrochloric acid, followed by a reaction with 6-chloro-1-hexanol and then with methacryloyl chloride. ^{1}H NMR (300 MHz, $CDCl_3$, 25 °C, TMS): δ = 1.17 (t, 3H), 1.36−1.42 (m, 4H), 1.64 (t, 2H), 1.74 (t, 2H), 1.88 (s, 3H), 3.97 (q, 2H), 4.03−4.12 (m, 4H), 5.48 (d, 1H), 6.04 (d, 1H), 6.92 (m, 4H), 7.78 (m, 4H). DSC: mp 106 °C. UV−vis (chloroform): λ_{max}/nm = 360.

6-(4-Cyano-4′-biphenoxy)hexyl methacrylate (M6CB). M6CB was prepared by the Schötten-Baumann reaction between methacryloyl chloride and (4-cyano-4′-biphenyloxy) hexyl-1-ol. ^{1}H NMR (300 MHz, $CDCl_3$, 25 °C, TMS): δ = 1.45−1.55 (m, 4H), 1.71 (t, 2H), 1.82 (t, 2H), 1.92 (s, 3H), 3.98 (q, 2H), 4.15 (q, 2H), 5.53 (d, 1H), 6.08 (d, 1H), 6.95 (d, 2H), 7.52 (m, 2H), 7.60−7.68 (m, 4H). DSC: mp 74 °C. UV−vis (chloroform): λ_{max}/nm = 298.

Homopolymer PM6AB. $Cu^{I}Cl$ (10 mg, 0.1 mmol) and M6AB (1.64 g, 4.0 mmol) were mixed in a 25-mL ampule, degassed and filled with argon. HMTETA (23.0 mg, 0.1 mmol) and EBrIB (19.5 mg, 0.1 mmol) in anisole (10.0 mL) were added through a syringe. The mixture was degassed by three freeze−pump−thaw cycles, sealed under vacuum, and placed in an oil bath preheated at 80 °C for 24 h. Then the solution was passed through a column (silica gel) with THF as eluent and the filtrate was precipitated into hot methanol at 60 °C. The polymer was collected and refluxed in hexane to remove unreacted M6AB. Then PM6AB of 0.92 g (yield, 56%) was obtained as a yellow solid. The number-average molecular weight (M_n) and the polydispersity index (M_w/M_n) were obtained as 10 000 and 1.21, respectively. ^{1}H NMR ($CDCl_3$): δ = 7.78 (d, 2H), 6.88 (d, 2H), 3.96−3.85 (m, 6H), 2.61 (m, 2H), 1.17−0.87 (m, 15H). UV−vis (chloroform): λ_{max} /nm = 360.

Macroinitiator PMMA−Br. After MMA (11.0 g, 110 mmol), $Cu^{I}Cl$ (0.099 g, 1.0 mmol), HMTETA (0.23 g, 1.0 mmol), and EBrIB (0.195 g, 1.0 mmol) were added in a Pyrex tube ampule under argon, the mixture was degassed by three freeze−pump−thaw cycles and sealed under vacuum, then stirred for 30 min at room temperature. The reaction was carried out in a preheated oil bath at 100 °C. After 20 min, the reaction mixture was cooled in cold water. The solid product was dissolved in THF and passed through a silica gel column to remove the catalyst, and the solvent was removed. The product was precipitated by pouring the concentrated solution into a large excess of methanol. Then the PMMA−Br was purified by reprecipitation from THF into methanol and dried under vacuum until reaching a constant weight. Polymer yield (6.6 g, 60%) was determined by gravimetry. M_n = 12 000, M_w/M_n = 1.12.

Diblock Copolymer PM−AB22. PMMA−Br (1.2 g, 0.1 mmol), $Cu^{I}Cl$ (9.9 mg, 0.1 mmol) and M6AB (2.87 g, 7.0 mmol) were mixed in a 50 mL ampule, degassed and filled with argon. HMTETA (23.0 mg, 0.1 mmol) in anisole (30.0 mL) was added. The mixture was degassed by three freeze−pump−thaw cycles and sealed under vacuum, placed in an oil bath preheated at 80 °C for 24 h. Then the solution was passed through a column (silica gel) with THF as eluent and the filtrate was precipitated into hot methanol (60 °C). The copolymer was collected and dried. Yield: 2.36 g (58%). M_n = 24 000, M_w/M_n = 1.06. UV−vis (chloroform): λ_{max}/nm = 360.

The other diblock copolymers and diblock random copolymers were prepared by a similar method. The mesogen constitution was controlled by the feed ratio of the mesogenic monomers (M6AB, M6CB) to the macroinitiator PMMA−Br.

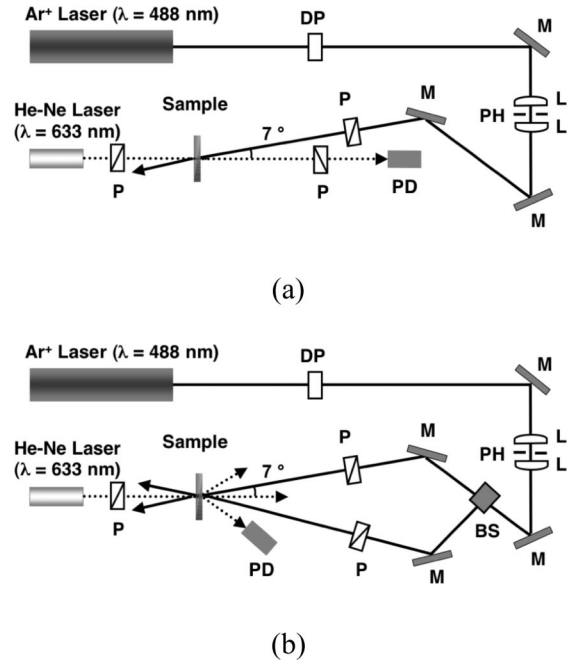

Figure 1. Optical setups used in this study: (a) photoinduced alignment; (b) holographic recording with Ar^+ laser beams. Key: A, analyzer; BS, beam splitter; L, lens; M, mirror; P, polarizer; PD, photodiode; DP, depolarizer; PH, pinhole.

Random Copolymer r-AB24. The random copolymer *r*-AB24 was prepared by radical polymerization in DMF by using AIBN as an initiator. M6AB (1.44 g, 3.5 mmol), MMA (0.65 g, 6.5 mmol) and AIBN (25 mg, 0.1 mmol) were dissolved in dry DMF (10 mL) and placed in a polymerization tube. After three freeze−pump−thaw cycles, the tube was sealed under high vacuum. Then the tube was kept at 60 °C for 48 h. The resulting solution was poured into a large excess of methanol with vigorous stirring to precipitate the polymer. The random copolymer *r*-AB22 was purified by reprecipitation from THF into methanol and dried under vacuum for 48 h to yield 1.29 g (62%). M_n = 24 000, M_w/M_n = 1.66. UV−vis (chloroform): λ_{max}/nm = 360.

2.4. Film Preparation and Microphase Separation. The polymer films were prepared by spin-coating their chloroform solutions on clean glass substrates. The film thickness of about 600 nm was estimated with a surface profiler (Veeco Instruments Inc., Dektak 3ST). After the solvent was removed at room temperature, the films were annealed at 160 °C in a vacuum oven for 24 h. Both the heating and cooling rates were controlled at 0.5 °C/min. The microphase-separated structures were measured with an AFM in a tapping mode at room temperature.

2.5. Photoinduced Alignment. The photoinduced change in refractive index of polymer films was investigated by the optical setup shown in Figure 1a. A linearly s-polarized beam from an Ar^+ laser (488 nm) at an intensity of 100 mW/cm^2 was incident to the polymer films at an angle of 7°. The intensity of the probe beam from a He−Ne laser (NEC, GLS5360 for a laser head; NEC, GLS5360 for a laser power supply NEC) at 633 nm transmitted through a pair of crossed polarizers, with the sample film between them, was measured with a photodiode. To investigate the photoinduced change in the alignment of AZ moieties in films, the polarized absorption spectra were measured before and after irradiation. The order parameter (S) was calculated by the following equation:

$$S = (A_\perp - A_{||})/(A_\perp + 2A_{||}) \quad (1)$$

Here $A_\perp$ and $A_{||}$ are the absorbance of UV−vis spectra measured with polarized beams perpendicular and parallel to the polarization direction of the laser beam, respectively.[11]

Scheme 1. Synthetic Schemes of the Homopolymers, the Random Copolymer, the Diblock Copolymers, and the Diblock Random Copolymers

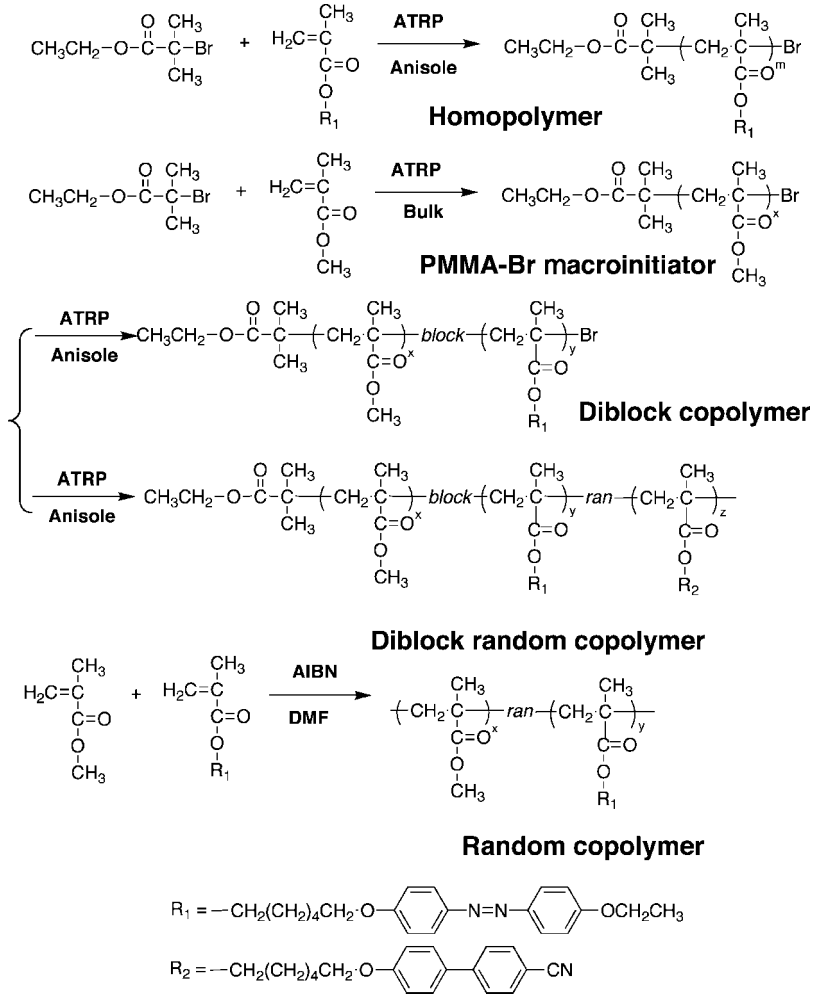

2.6. Grating Recording. Figure 1b illustrates the optical setup for recording holographic gratings in spin-coated films.[12] Two linearly s-polarized beams at 488 nm with an equal intensity of 50 mW/cm^2 (or 250 mW/cm^2 for diblock random copolymers) from an Ar+ laser were used as writing beams. The interference beams were crossed on the film surface at an incident angle of 7°, leading to an interference pattern with a fringe spacing of 2.0 μm according to $\Lambda = \lambda/(2 \sin \theta)$, where λ and θ are the wavelength and the incident angle of the writing laser beams, respectively. The two beams were collimated to a diameter of about 2.0 mm on the film surface. A He−Ne laser beam at 633 nm was used as a reading beam as the copolymer films have little absorption at this wavelength. The grating formation was confirmed in real time by monitoring the intensity of the first-order diffraction beam with a photodiode in a transmission mode. The diffraction efficiency of gratings was defined as $\eta = I_1/I_0$, where I_1 is the intensity of the first-order diffraction beam, and I_0 represents the intensity of the transmitted beam through the film without the writing beams, respectively. The reading beam was also normal to the film surface.

3. Results and Discussion

3.1. Synthesis. The synthetic schemes of all the polymers are shown in Scheme 1. To prepare well-defined molecular structures, it is necessary to synthesize BCs with a narrow molecular-weight distribution, which is normally realized by living polymerization. Generally, ATRP has been regarded as one of the controlled/living radical polymerizations,[13] which has been widely applied to synthesize monodispersed macroinitiator PMMA−Br in solutions.[14] Organic solvents are often used to control the heat of reaction released in the polymerization, while a longer reaction time is required. To prepare the well-defined macroinitiator within a short time, a bulk ATRP reaction of MMA was carried out by carefully adjusting the feed molar ratio of monomer/initiator ([MMA]/[EBrIB]$_0$ = 110), reaction temperature (100 °C), reaction time (20 min) and by cooling the final reaction mixture quickly in water (0 °C) to stop the reaction. PMMA−Br with a well-designed molecular weight (M_n = 12 000) and a narrow polydispersity (M_w/M_n = 1.12) was successfully obtained. About 120 repeated units of MMA were estimated from ^{1}H NMR and GPC (PMMA$_{120}$−Br).

The obtained PMMA$_{120}$−Br showed good reactivity to an ATRP reaction of the monomer (M6AB) or monomer mixture (M6AB and M6CB) in anisole. A series of PMMA-based diblock copolymers and diblock random copolymers were prepared by controlling the feed ratios of the monomers to the macroinitiator. All the GPC curves of the obtained BCs exhibited a unimodal peak, indicating their controlled molecular structures and narrow molecular weight distributions. Their specifically designed chemical constitutions could be estimated from their ^{1}H NMR spectra, which are summarized in Table 1. For comparison, a random copolymer (*r*-AB24) was also prepared by a typical radical polymerization.

Figure 2 gives the typical UV−vis spectra of the macroinitiator PMMA−Br, the diblock copolymer PM−AB66 and the diblock random copolymer PM−AB3CB17 in chloroform. No obvious absorption peak appeared at 250−650 nm in the UV−vis spectrum of PMMA−Br, whereas two and three

Table 1. Summary of the Materials Prepared in this Study[a]

sample	abbreviation	M_n	M_w/M_n	[AB]:[CB]:[MMA] (mol %)	phase transition temperature (°C)
homopolymers	PMMA−Br	12 000	1.12		G118 I
	PM6AB	10 000	1.21		G 56LC155I
diblock copolymers	PM−AB9	19 000	1.04	9:0:91	G105 I
	PM−AB22	24 000	1.06	22:0:78	G 94LC147I
	PM−AB66	40 000	1.07	66:0:34	G 89LC154I
diblock random copolymers	PM−AB3CB17	30 000	1.09	3:17:80	G 64LC133I
	PM−AB8CB16	34 000	1.07	8:16:76	G 69LC138I
	PM−AB11CB12	35 000	1.07	11:12:77	G 69LC164I
random copolymer	*r*-AB24	24 000	1.66	24:0:76	G 82 I

[a] Key: G, glassy; LC, liquid crystal; I, isotropic.

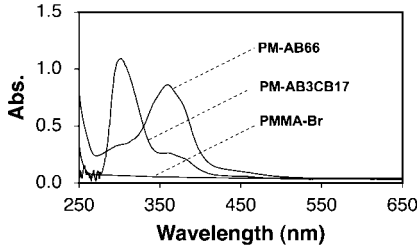

Figure 2. UV−vis spectra of the macroinitiator PMMA−Br, the diblock copolymer PM−AB66 and the diblock random copolymer PM−AB3CB17 in chloroform.

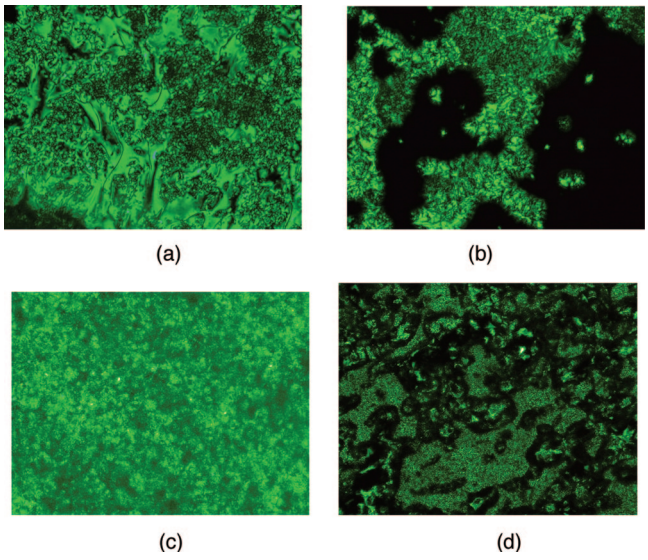

Figure 3. Typical POM images (magnification × 500) of PM6AB (a), PM−AB22 (b), PM−AB66 (c), and PM−AB3CB17 (d).

maximum peaks were observed in those of PM−AB66 and PM−AB3CB17, respectively. Two peaks at almost the same bands for the two copolymers are due to the absorption of the AZ. One band is around 360 nm owing to the $\pi-\pi^*$ transition, and the other band at 460 nm is attributed to the $n-\pi^*$ transition.[15] The peak at around 300 nm was observed only in PM−AB3CB17, attributed to the $\pi-\pi^*$ transition of the CB, whose absorbance was far higher than that of the AZ because of its relative higher content.

3.2. Thermal Analysis. The thermal properties of all the obtained polymers were investigated by DSC and POM. Figure 3 shows the typical POM images of the homopolymer PM6AB and the LCBCs. All the POM pictures gave Schlieren textures, a typical texture of nematic LC phases. Among them, two LCBCs (PM−AB22 and PM−AB3CB17), exhibited incontinuous textures in Figure 3b,d because of relative low contents of mesogenic groups. Upon annealing at 160 °C, such LC textures as seen in Figure 3b,d disappeared, while no obvious change occurred in those of Figure 3a,c. Similar to our previous results,[5d] the thermally enhanced microphase separation is responsible for the undetected LC textures as the mesogenic blocks have been confined into nanoscale phase domains, whose size is beyond the limitation of the present POM resolution. Other two diblock random copolymers showed similar behavior to PM−AB3CB17.

The diblock copolymer PM−AB9 exhibited an amorphous state owing to its far lower AZ content. Although the random copolymer *r*-AB24 has a similar AZ composition to that of the diblock copolymer PM−AB22, it showed no LC phase. In a diblock copolymer with a well-defined structure, the AZ block is incompatible with the PMMA segment. Thus microphase separation occurs in which the AZ mesogens segregate together, enabling to form an LC order in the local area. Although a random copolymer shows a statistical molecular structure, in which AZ moieties are homogeneously dispersed in PMMA, no microphase separation can be obtained as the AZ and MMA are completely miscible, resulting in an amorphous phase. It seems that a BC shows an LC phase more easily than a random copolymer with a similar low content of mesogens. The acquired LC property might endow the BC with advanced performances such as physical anisotropy, self-organization, long-range ordering and molecular CM.[2]

3.3. Microphase Separation. To measure the microphase-separated domains in thin films of the obtained BCs, AFM images in a tapping mode were adopted. As shown in Figure 4, the nanostructures can be clearly observed in the annealed films, owing to the difference in elastic modulus between the amorphous PMMA and the mesogenic phases at room temperature.[9] It is well-known that BCs self-assemble into a range of different nanostructures, whose size can be controlled by adjusting the chain length (molecular weight), chemical functionality, volume fraction of each block.[3] In the present PMMA-based BCs, the AZ block formed either separated (Figure 4a,b) or continuous (Figure 4c) phases depending on its relative content in the block copolymers.[16] The possible microphase structures of the BCs are depicted in Figure 4. Similar to Figure 4a,b, the mesogenic blocks also formed the minority phases in all the obtained diblock random copolymers because of their lower compositions of mesogens. The mesogens were confined in the minority phase with a nanoscale dispersion in the continuous phase of the transparent PMMA substrate, enabling to eliminate the scattering of visible light. This could improve the optical performance of the BC films. Different from the BCs with well-defined structures, no obvious microphase separation in the film of random copolymer *r*-AB24 was detected by AMF because of its random and unspecific molecular structure, in which the AZ and MMA are completely miscible.

3.4. Photoinduced Birefringence. Upon annealing, the photoinduced alignment in films was examined with a linearly polarized beam at 488 nm. The transmittance (T) of a He−Ne laser beam at 633 nm with a low intensity as a probe beam was measured simultaneously during irradiation through two crossed polarizers with the sample films between them. Generally, T is

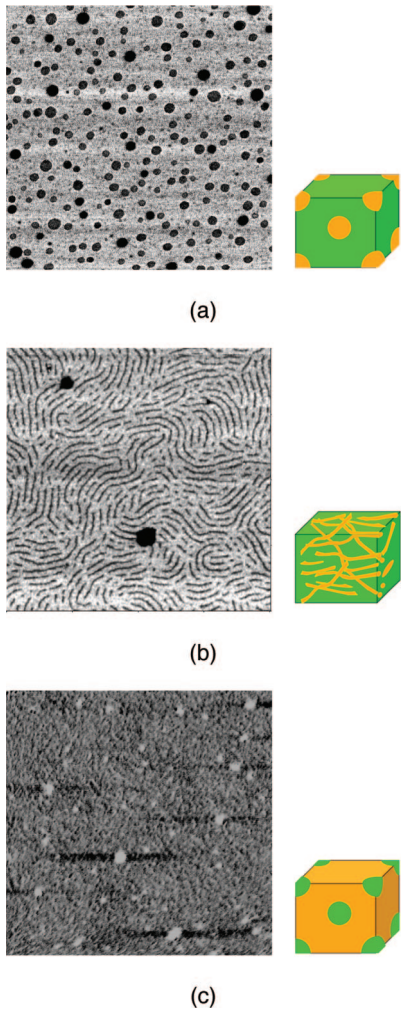

Figure 4. Representative AFM phase images and their corresponding possible microphase structures of diblock copolymers. Key: (a) PM−AB9; (b) PM−AB22; (c) PM−AB66. The data scale is 1 μm. The yellow part is a mesogenic block, while the green one is a PMMA phase.

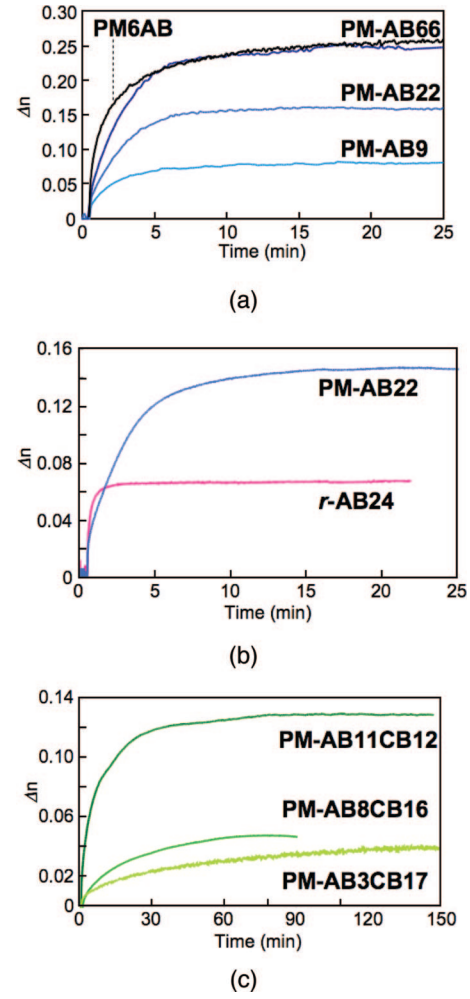

Figure 5. Photoinduced change in birefringence (Δn) of thin films of the obtained polymers.

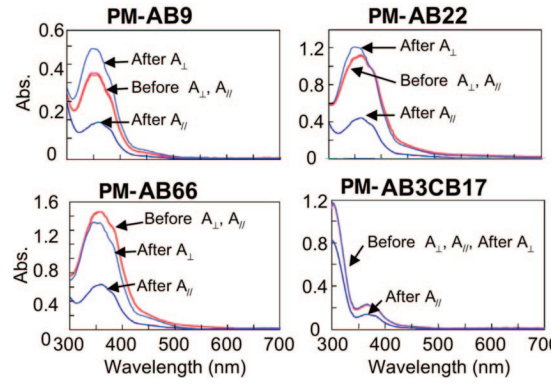

Figure 6. Typical polarized UV−vis absorption spectra of the block copolymers. $A_{||}$ and $A_{\perp}$ donate absorption parallel and perpendicular to the polarization direction of actinic light, respectively.

defined by $T = \sin^2(\pi d\Delta n/\lambda)$, where d is the film thickness, Δn is the photoinduced birefringence, and λ is the wavelength of the probe light. Figure 5 shows the photoinduced change in LC alignment. All the obtained polymers can be subjected to photoinduced alignment to generate birefringence, but they showed different behavior. For the diblock copolymers, the saturated value of Δn increased with the AZ content. As the AZ block constitutes a continuous phase in PM−AB66, it showed a similar performance to the homopolymer, and the Δn of 0.24 was obtained. A lower Δn of 0.14 was observed in PM−AB22 because the AZ mesogens were confined in a minority phase. With the lowest content of the AZ block, PM−AB9 exhibited the lowest Δn of 0.07. Considering the thermal properties, the amorphous phase of PM−AB9 accounts for the little Δn. Similarly, the random copolymer *r*-AB24 exhibited a far lower value of Δn than the LCBC PM−AB22 with almost the same AZ content as seen in Figure 5b. Therefore, the BC has superior advantage over a statistically random copolymer because the anisotropic LC phase can be easily obtained in BC with a lower mesogenic composition than that in the latter one. For the three diblock random copolymers, all the mesogenic blocks formed separated phases dispersed in the continuous PMMA substrate, and their photoinduced alignment was performed in the confined nanospaces. As the Δn was obtained by the photoinduced alignment of AZs and their triggered orientation of photoinert CBs by molecular CM, a much longer time of irradiation was needed than that of the diblock copolymers with AZs as only mesogens (Figure 5c).

Before irradiation, all the transparent films showed isotropy as no alignment of mesogens was obtained by annealing and microphase separation. After photoinduced alignment, all the irradiated films showed large anisotropy in their polarized UV−vis absorption spectra (Figure 6). For the homopolymer PM6AB and all the diblock copolymers, large anisotropic absorption was observed at the band of about 360 nm, owing to the homogeneous alignment of AZs. An order parameter of about 0.35 was obtained from eq 1. On the other hand, two

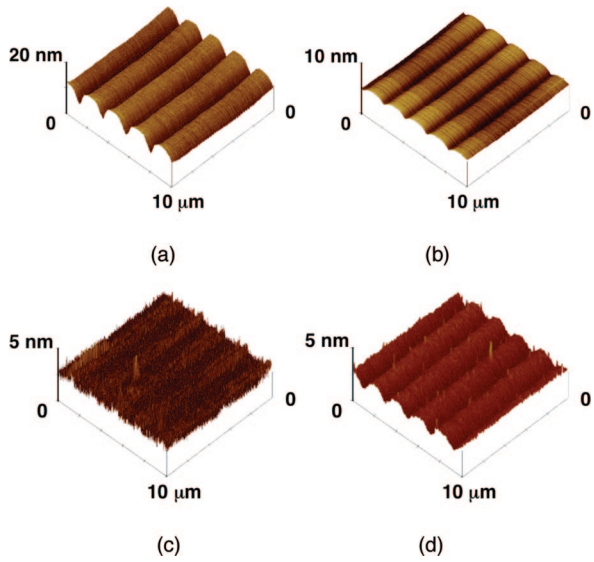

Figure 7. 3D AFM images of holographic gratings recorded in polymer films. Key: (a) PM−AB66; (b) PM−AB22; (c) PM−AB9; (d) PM−AB3CB17.

anisotropic absorption peaks were observed at the bands of about 300 and 360 nm in PM−AB3CB17, attributed to the $\pi-\pi^*$ transitions of AZs and CBs, respectively. Generally, AZs are well-known for their photoinduced alignment with transition moments almost perpendicular to the polarization direction of the actinic light.[2,15] In the diblock random copolymers, although the CBs do not absorb the actinic light at 488 nm, they can be aligned together with the AZs because of the phototriggered molecular CM, which is similar to that of the well-defined triblock copolymer.[9] Considering the polarized UV−vis absorption in Figure 6, it is reasonable to infer that the orientation of the CBs is also normal to the polarization direction of the laser light.

3.5. Holographic Recording. Then holographic grating experiments were carried out in the microphase-separated copolymer films. All the gratings belong to the Raman−Nath type according to the dimensionless Q-parameter evaluated from eq 2.

$$Q = \frac{2\pi\lambda_R d}{n\Lambda^2} \tag{2}$$

where λ_R is the wavelength of the readout beam, d is the thickness of the film, n is the refractive index, and Λ is the fringe spacing.[17]

After the grating formation, a surface-relief structure of about 14 nm was observed in the three-dimensional (3D) AFM image of PM−AB66 (Figure 7a). Such a surface modulation is smaller than that of the homopolymer PM6AB (about 70 nm),[18] which might be attributed to the microphase-separated structures of BCs. Even though the photoinduced alignment of PM−AB66 is seldom influenced by microphase separation with AZs in a continuous phase, the photoinduced mass transportation, which is necessary for the formation of SRGs,[15] seems to be partly confined because of a higher T_g (94 °C) than that of PM6AB (56 °C). Accompanying with the SRG formation, a refractive-index grating (RIG) structure with the same grating constant of 2.0 μm to that of the SRG was clearly observed in its POM picture shown in Figure 8. The periodic bright and dark stripes were alternately formed along the grating vector, which periodically disappeared when rotating the grating sample by 45°. This demonstrates that the photoinduced change in alignment of AZs was successfully brought about in the bright stripes, leading to

Figure 8. POM picture of the holographic grating recorded in the film of PM−AB66. The grating was recorded at $\theta = 7°$, leading to a fringe spacing of 2 μm. Key: A, analyzer; P, polarizer.

the periodic change in refractive index. Based on the analytical results, the bright areas of the interference pattern correspond to the bright stripes of the RIG images with AZs in an alignment state, which are the trenches of the SRG. On the other hand, the dark areas correlate with dark stripes of the RIG images with AZs in random, which correlate with the peaks of the SRG. Such structures are contrary to our previous results of AZ-containing LCBCs with pretreatment beforehand.[5b] Similarly, the RIG structure was stable under room light as the BC is in its glassy state.

A little surface modulation of about 6 nm was observed in the 3D AFM picture of PM−AB22 shown in Figure 7b. As the AZ block formed a separated phase domain in the microphase separation, the photoinduced mass transfer was greatly confined by the glassy PMMA. Although a nematic LC phase-transition peak was observed in its DSC curve, no RIG structures were obtained by POM. Figure 7c shows little surface relief in the grating recorded in PM−AB9, indicating that the photoinduced mass transfer in the film was almost completely prohibited by the microphase separation. Recently, the lack of SRG has been reported on amorphous PS-based BCs with AZs in a minority phase.[8c] Such a repressive function of SRG by microphase separation has potential applications in volume hologram.[8b] Since the photoinduced CM between AZs and CBs was phototriggered in the nanoscaled separated phase, the diblock random copolymers showed an alike performance of confinement effect of SRG. As shown in Figure 7d, little surface modulation was detected. Besides, the RIG structure cannot be clearly obtained by POM.

3.6. Modulation of Refractive Index. It is noteworthy that the surface modulation of SRG in the BC films was far smaller than the film thickness, and the contribution of the surface relief to the spatial modulation of the refractive index can be almost negligible. Then the modulation of refractive index ($\Delta n'$) could be evaluated according to Kogelniks theory by the following equation,

$$\eta = \left(\frac{\pi d \Delta n'}{\lambda}\right)^2 \tag{3}$$

where d and λ are the film thickness and wavelength of the reading beam, respectively.[19] The estimated results are given in Figure 9.

Different from the surface-modulation behavior, PM−AB66 showed a similar performance of $\Delta n'$ to that of the homopolymer PM6AB, and about 0.058 was obtained after recording for 30 min. Thanks to the large refractive-index modulation, which leads to a different phase retardation of about 35 nm between the bright and dark areas of the interference pattern, the RIG structure can be clearly observed in the POM picture shown in Figure 8. In Figure 9a, the other two BCs with AZs in the minority phases (PM−AB22 and PM−AB9) exhibited a quick response to the holographic recording because the molecular CM is interrupted by the continuous phase of glassy PMMA, leading to a lower $\Delta n'$ of 0.03 and 0.01, respectively. Because

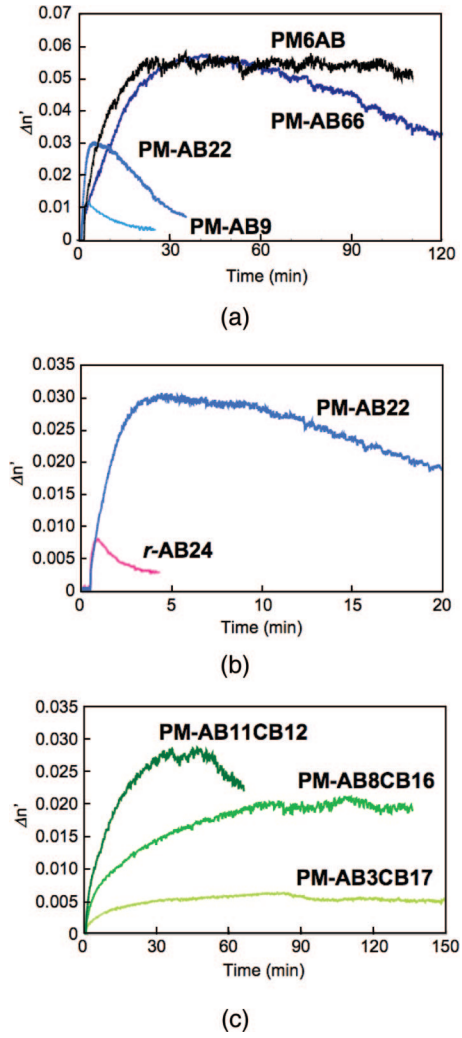

Figure 9. Photoinduced change in refractive index as a function of the holographic recording time.

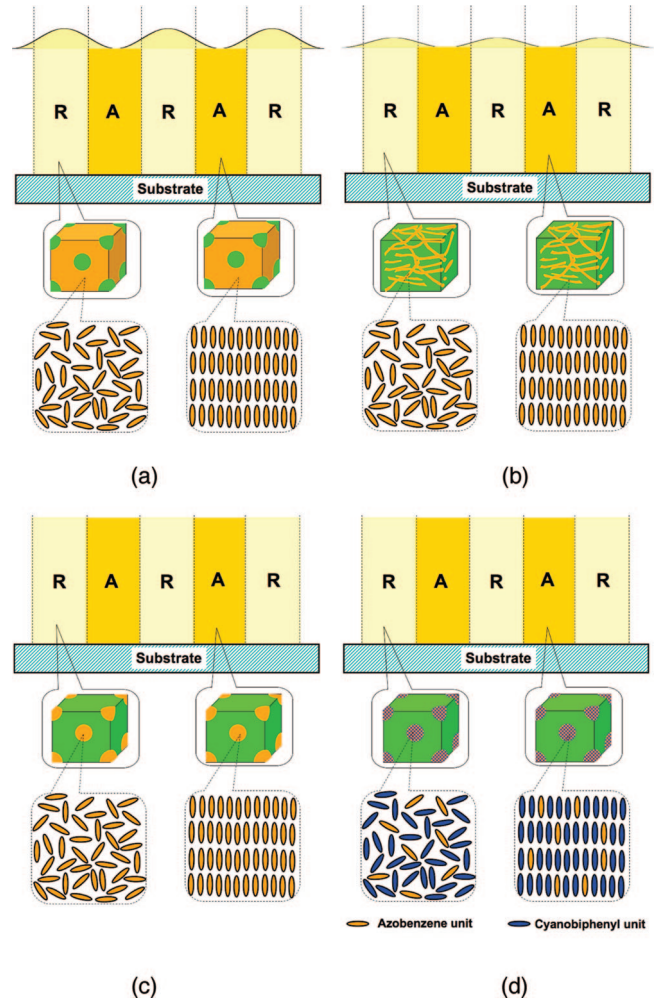

Figure 10. Plausible schemes of mesogens and microphase separation in the grating structures recorded in the block copolymer films: (a) diblock copolymer PM−AB66; (b) PM−AB22; (c) PM−AB9; (d) diblock random copolymer. Key: A, aligned; R, random.

of the amorphous phase of the random copolymer *r*-AB24, a value of 0.008 was obtained for Δn′, which is far lower than that of PM−AB22 with a similar AZ content (Figure 9b). For the diblock random copolymers, the photoinduced nanoscale CM in the bright areas of the recording interference pattern is a driver to induce Δ*n*′, whereas no phototriggered motion occurred in the dark area. As the photoinduced alignment of AZs and the following CM between the ordered AZs and random CBs are involved, a higher irradiation intensity and a long recording time are required to obtain a larger value of Δ*n*′ as shown in Figure 9c.

Figure 10 gives the plausible schematic illustrations of the mesogens and microphase separation in holographic gratings recorded in the BCs. Both a SRG and a RIG are recorded in PM−AB66 with AZs in the majority phase (Figure 10a). A smaller surface modulation and a lower Δn′ are obtained in PM−AB22 with a lower content of AZs (Figure 10b). Little surface relief and a RIG are demonstrated in Figure 10c,d for PM−AB9 or diblock random copolymers with mesogenic groups in the minority phases. The photoinduced mass transportation has been thoroughly prohibited by microphase separation, which is responsible for the obtained gratings without surface modulation. Either the photoinduced alignment of AZs or the phototriggered CM between AZs and CBs occurs in the bright area of the recording interference pattern, which is responsible for the formation of Δn′.

4. Conclusions

A series of PMMA-based diblock copolymers and diblock random copolymers with well-defined structures were prepared by ATRP. By controlling the relative contents in the copolymers, the mesogenic blocks constituted either a majority phase or a minority phase upon microphase separation. All the BCs showed photoinduced alignment and were subjected to holographic gratings; however, they showed different behavior because of their varied mesogenic content. PM−AB66 with AZs in the majority phase exhibited a similar performance of Δn and Δn′ to that of the homopolymer PM6AB. On the other hand, the photoinduced mass transportation was partly hampered by the microphase-separated structures in a glassy state, resulting in a lower surface relief than that of PM6AB. With a lower AZ content, PM−AB22 demonstrated a surface relief of about 6 nm and Δ*n*′ of 0.03. When the mesogenic blocks formed a separated microphase in PM−AB9 or diblock random copolymers, either the photoinduced alignment of AZs or the phototriggered CM between AZs and photoinert CBs accounted for the generation of Δ*n*′, whereas little surface relief was observed because the photoinduced mass transportation has been almost completely prohibited by the continuous phase of PMMA in a glassy state. The BCs have superior advantage over the random copolymers because the anisotropic LC phase can be easily obtained with a lower mesogenic content than that of the statistical copolymers. Besides, confining the photoinduced

alignment of AZs or the phototriggered molecular CM between AZs and CBs in nanoscale mesogenic domains dispersed in the majority phase of PMMA, a large Δn of about 0.02−0.12 was obtained, whereas the scattering of visible light was eliminated, indicating their potential applications as recording media for volume holograms, which are underway in our laboratory.

References and Notes

(1) (a) Walther, M.; Finkelmann, H. *Prog. Polym. Sci.* **1996**, *21*, 951. (b) Mao, G.; Ober, C. K. *Acta Polym.* **1997**, *48*, 405. (c) Poser, S.; Fischer, H. *Acta Polym.* **1996**, *47*, 413. (d) Lee, M.; Cho, B. K.; Zin, W. C. *Chem. Rev.* **2001**, *101*, 3869.

(2) (a) Demus, D.; Goodby, J.; Gray, G. W.; Spiess, H.-W.; Vill, V. *In Handbook of Liquid Crystals*; Wiley-VCH: Weinheim, Germany, 1998; (b) Ikeda, T.; Tsutsumi, O. *Science* **1995**, *268*, 1873. (c) Ikeda, T. *J. Mater. Chem.* **2003**, *13*, 2037.

(3) (a) Bates, F. S.; Fredrickson, G. H. *Phys. Today* **1999**, *52*, 32. (b) Fasolka, M. J.; Mayes, A. M. *Annu. Rev. Mater. Res.* **2001**, *31*, 323. (c) Ikkala, O.; Brinke, G. T. *J. Chem. Soc., Chem. Commun.* **2004**, 2131. (d) Bockstaller, M. R.; Mickiewicz, R. A.; Thomas, E. L. *Adv. Mater.* **2005**, *17*, 1331.

(4) (a) Tian, Y.; Watanabe, K.; Kong, X.; Abe, J.; Iyoda, T. *Macromolecules* **2002**, *35*, 3739. (b) Yu, H. F.; Iyoda, T.; Ikeda, T. *J. Am. Chem. Soc.* **2006**, *128*, 11010. (c) Yu, H. F.; Li, J. Z.; Ikeda, T.; Iyoda, T. *Adv. Mater.* **2006**, *18*, 2213. (d) Yu, H. F.; Shishido, A.; Li, J. Z.; Kamata, K.; Iyoda, T.; Ikeda, T. *J. Mater. Chem.* **2007**, *17*, 3485.

(5) (a) Morikawa, Y.; Nagano, S.; Watanabe, T.; Kamata, K.; Iyoda, T.; Seki, T. *Adv. Mater.* **2006**, *18*, 883. (b) Yu, H. F.; Okano, K.; Shishido, A.; Ikeda, T.; Kamata, K.; Komura, M.; Iyoda, T *Adv. Mater.* **2005**, *17*, 2184. (c) Yu, H. F.; Shishido, A.; Ikeda, T.; Iyoda, T. *Macromol. Rapid Commun.* **2005**, *26*, 1594. (d) Yu, H. F.; Shishido, A.; Iyoda, T.; Ikeda, T. *Macromol. Rapid Commun.* **2007**, *28*, 927.

(6) (a) Osuji, C.; Ferreira, P. J.; Mao, G.; Ober, C. K.; Vander Sande, J. B.; Thomas, E. L. *Macromolecules* **2004**, *37*, 9903. (b) Hamley, I. W.; Castelletto, V.; Lu, Z. B.; Imrie, C. T.; Itoh, T.; Al-Hussein, M. *Macromolecules* **2004**, *37*, 4798. (c) Tomikawa, N.; Lu, Z.; Ioth, T.; Imrie, C. T.; Adachi, M.; Tokita, M.; Watanabe, J. *Jpn. J. Appl. Phys.* **2005**, *44*, L711.

(7) (a) Wu, Y.; Natansohn, A.; Rochon, P. *Macromolecules* **2004**, *37*, 6090. (b) Cui, L.; Yan, X. H.; Liu, G. J.; Zhao, Y. *Macromolecules* **2004**, *37*, 7097. (c) Tong, X.; Cui, L.; Zhao, Y. *Macromolecules* **2004**, *37*, 3101.

(8) (a) Häckel, M.; Kador, L.; Kropp, D.; Frenz, C.; Schimidt, H. *Adv. Func. Mater.* **2005**, *15*, 1722. (b) Häckel, M.; Kador, L.; Kropp, D.; Schimidt, H. *Adv. Mater.* **2007**, *19*, 227. (c) Frenz, C.; Fuchs, A.; Schimidt, H.; Theissen, U.; Haarer, D. *Macromol. Chem. Phys.* **2004**, *205*, 1246.

(9) Yu, H. F.; Asaoka, S.; Shishido, A.; Iyoda, T.; Ikeda, T. *Small* **2007**, *3*, 768.

(10) Breiner, T.; Kreger, K.; Hagen, R.; Hackel, M; Kador, L.; Mu1ller, A.; Kramer, E.; Schmidt, H. *Macromolecules* **2007**, *40*, 2100.

(11) Neff, V. D. In *Liquid Crystals and Plastic Crystals*; Gray, G. W.; Winsor, P. A., Eds.; Ellis Horwood: U. K. Chichester, 1974; Vol. *2*, p 231.

(12) Yamamoto, T.; Hasagawa, M.; Kanazawa, A.; Shiono, T.; Ikeda, T. *J. Phys. Chem. B* **1999**, *103*, 9873.

(13) Matyjaszewski, K.; Xia, J. H. *Chem. Rev.* **2001**, *101*, 2921.

(14) (a) Grimaud, T.; Matyjaszewski, K. *Macromolecules* **1997**, *30*, 2216. (b) Karanam, S.; Goossens, H.; Klumperman, B.; Lemstra, P. *Macromolecules* **2003**, *36*, 8304.

(15) Natansohn, A.; Rochon, P. *Chem. Rev.* **2002**, *102*, 4139.

(16) Park, C.; Yoon, J.; Thomas, E. L. *Polymer* **2003**, *44*, 6725.

(17) Collier, R. J.; Burckhardt, C. B.,; Lin, L. H. *Optical Holography*; Academic Press: New York, 1971.

(18) Yamamoto, T.; Hasegawa, M.; Kanazawa, A.; Shiono, T.; Ikeda, T. *J. Mater. Chem.* **2000**, *10*, 337.

(19) Hicher, H. J.; Gunther, P.; Pohl, D. W. *Laser Induced Dynamic Grating*; Springer-Verlag: Berlin, 1986.

MA801077G